ELSEVIER

Surface Science 347 (1996) 63–79

surface science

The growth of aluminum on a rhenium ($10\bar{1}0$) surface

M. Parschau, K. Christmann *

Institut für Physikalische und Theoretische Chemie der Freien Universität Berlin, D-14195 Berlin, Germany

Received 26 June 1995; accepted for publication 2 October 1995

Abstract

Al thin films were deposited at 873 K on a Re($10\bar{1}0$) surface and examined by means of low-energy electron diffraction (LEED), Auger electron spectroscopy (AES), thermal desorption spectroscopy (TDS), and work function ($\Delta\Phi$) measurements. In the submonolayer range ($0<\Theta_{Al}<0.6$), we find two Al LEED structures, a p(3×1) at $\Theta_{Al}\approx0.3$, and a p(2×1) at $\Theta_{Al}\approx0.5$. In the same coverage range, a single TD state denoted as β_3 appears having a desorption energy of 440 kJ/mol. Close to $\Theta_{Al}\approx1$ another (2×1) LEED phase and a second TD state (β_2) develop which exhibits a desorption energy of $\sim$375 kJ/mol. This (2×1) phase is then replaced up to $\Theta_{Al}\approx2$ by a clear c(2×2) phase, followed by a p(2×2) and another c(2×2) structure at still higher Al coverages. In this multilayer range, the TD spectra are dominated by a single desorption state denoted as β_1 which reflects a fractional-order kinetics and yields an activation energy of $\sim$345 kJ/mol. The deposition of Al reduces the Re work function by $\sim$1.2 eV. A plot of the Re versus Al Auger intensity reveals a clear break at $\Theta_{Al}\approx1$ and a less pronounced break around $\Theta_{Al}\approx2$, while for higher Al coverages the Re AES intensity decays unspecifically, which suggests deviations from a plain layer-by-layer growth. Up to $\sim$8 deposited monolayers the structure of the Al film is determined by the crystallography of the Re($10\bar{1}0$) surface and by relaxation processes to overcome the misfit.

Keywords: Aluminum; Auger electron spectroscopy; Growth; Low energy electron diffraction (LEED); Rhenium; Single crystal surfaces; Thermal desorption spectroscopy; Work function measurements

1. Introduction

Thin metal films have attracted a considerable interest for both fundamental and applied physical reasons. We only mention their use in materials science, physical electronics and the optics industry, or in the field of heterogeneous catalysis [1–4]. For a given film material both the physical and the chemical-catalytical properties very much depend upon its morphology (degree of dispersion, crystallographical long-range order etc.). A comprehensive status report concerning the atomic processes involved in thin film and crystal growth was recently given by Venables [5].

It is well known that in (hetero)epitaxy the substrate *geometry* and specific substrate-film interactions govern both the orientation of the film and its growth mechanism. According to Gebhardt [6] we understand the term epitaxy as a nucleation and growth relationship between two crystalline phases, which makes it possible for a crystalline phase g (guest crystal) to grow in a structure-dependent manner onto a given phase of given structure h (host crystal) developing, in general, an interfacial region which is chemically and structurally inhomogeneous. This definition of epitaxy includes all processes which occur at and near the

* Corresponding author.

SSDI 0039-6028(95)00959-0

phase boundary from the very beginning to the late stages of growth.

It may be useful in some cases to transfer conceptions and terms developed for gas chemisorption processes on surfaces to metal-on-metal epitaxy, and we may therefore consider the very first stages of heteroepitaxy as a kind of "adsorption" of foreign atoms on a metal surface, and we may define our system as consisting of an adsorbate (guest material) and a (host) substrate.

In the very low adsorbate concentration (coverage) range, strong adsorbate–substrate and adsorbate–adsorbate interactions may cause the formation of a boundary phase with long-range order, and, hence, the appearance of LEED superstructures. Adsorbate-induced surface reconstructions as well as chemical reactions (interdiffusion, alloying) are other examples of a specific interaction. Processes of this kind are often thermally activated (due to the required site exchange processes) and occur preferentially at elevated temperatures. In addition, they may depend on the dimensionality of the system. Even if there are large miscibility gaps in the bulk, alloying may take place in the surface region, and the thin alloy layers may exhibit novel and unexpected chemical and physical properties.

We have deposited thin aluminum layers on top of a rhenium $(10\bar{1}0)$ surface and focused on four major points: (i) Is it possible to grow *single crystalline* epitactic Al layers at elevated substrate temperatures? (ii) What is the electronic and geometric structure of the Al films? (iii) What is the growth mechanism? (iv) Is there a tendency for Al to diffuse into the bulk of Re and to form alloys? We note that the phase diagram of the Al–Re system which was reported by Savitskii et al. [7] exhibits a fairly complicated shape with a peritectic point and several intermetallic compounds, for example $ReAl_{12}$, $ReAl_2$, ReAl, and Re_3Al_2 – all these phases, however, exist only at temperatures well above 1000 K. The solubility of Al in solid Re is 2.8 mol% at ~2200 K, but drops significantly as one goes to lower temperatures. It is, therefore, most likely that there is actually very little solubility of Al in the Re surface in the temperature range of our experiment.

Rhenium is a very rare, but catalytically quite important chemical element, and it represents a very active component in Pt–Re catalysts used for technical reforming processes [8]. For experiments dealing with thin film deposition and characterization under ultra-high vacuum (UHV) conditions, Re is particularly convenient, because its extremely high melting point (~3443 K [9]) allows the thermal removal of almost any deposit material and, hence, helps to easily restore the conditions of a clean substrate surface simply by thermal desorption.

Refractory metals (Mo, W in particular) as substrates for thin film deposition have been repeatedly used in the past, and there exists a wealth of literature on this subject from which we only refer to the extensive work in the laboratory of E. Bauer where all kinds of metal deposits (preferentially the noble metals Cu, Ag and Au) were grown on Mo and W single crystal substrates [10–14]. Less work has been carried out with surfaces of the hexagonal-close-packed (hcp) metals rhenium and ruthenium; we recall papers from Bergholz and Gradmann [15], where thin Ni films were grown onto a Re(0001) surface and investigated with respect to their magnetic behavior, and a work by Rodriguez et al. [16] dealing with Cu and Pd deposition on Re(0001). Important recent contributions came from Campbell and Goodman, who reported on Al deposition onto Ru(0001) [17], and from Wu et al., who reinvestigated the same system Al on Ru(0001) [18]. To our knowledge, the anisotropic $Re(10\bar{1}0)$ surface (which exhibits a similar row-and-trough structure as the face-centered cubic (fcc) (110) surfaces) has not been used so far as a host surface for thin film deposition.

A likewise relatively scarce data base is available for thin aluminum films on single crystal metal surfaces. Here, we refer to work where Al was deposited onto the (densely-packed) (110) faces of the (bcc) refractory metals molybdenum [19,20] and tantalum [21]. In the early study by Jackson and Hooker [19] and Jackson et al. [21] especially the Al-induced LEED structures on Mo(110) [19] and Ta(110) [21] were examined, whereas in the more recent re-investigation of the Al-on-Mo(110)-system by Kołaczkiewicz et al. [20], combined LEED, AES, ELS, and $\Delta\Phi$ data were reported, whereby some of the earlier (structural) data were

superseded or re-interpreted. However, there is one parallel statement made in both investigations which we emphasize at this point: There is no evidence of Al–Mo alloy formation nor of noticeable solubility of Al in the Mo bulk obtained, not even at temperatures as high as 1300 K. Unfortunately, the situation concerning alloying is by no means consistent, because the recent papers on the Al-on-Ru(0001) system [17,18] both reported explicitly evidence of alloy formation, at least at elevated temperatures.

Our investigation of the Al-on-Re system was motivated by the interesting magnetic properties of Fe–Co–Al alloys [22], and it was our first goal to examine the deposition conditions for obtaining smooth single-crystalline layers of the pure components Al, Fe and Co, respectively, on top of a Re single crystal surface, and to characterize the geometric and electronic structure of these films in the submonolayer region. A report on the deposition and growth of cobalt films onto Re surfaces will follow [23]. While rhenium crystallizes in the hcp system and exhibits a metallic radius of 1.3775 Å, aluminum belongs to the fcc system with an atomic radius of 1.432 Å; i.e., Al atoms are about 4.5% larger than Re atoms which represents a moderate misfit in the lattice spacings [24]. It is, therefore, an interesting problem whether thin layers of Al will grow pseudomorphically with their structure being governed by the Re lattice parameters, or with their own characteristic bulk lattice constant.

2. Experimental

2.1. General set-up

Our experiments were performed in an all-metal ultra-high vacuum (UHV) chamber equipped with a four-grid optics for LEED and AES, a quadrupole mass spectrometer for TDS, and a Kelvin probe for $\Delta\Phi$ measurements. A base pressure of 10^{-10} mbar was routinely obtained by 600 ℓ/s oil-diffusion pump with a liquid-N_2 trap. During the operation of the Knudsen cell for Al deposition (see below) the pressure remained in the 10^{-10} mbar range.

2.2. Sample preparation and handling

The Re sample consisted of a lozenge-shaped waver with a thickness of $\sim$1 mm and an area of $\sim$1 cm^2; it was oriented by Laue X-ray diffraction to within 0.5° and cut by spark erosion before it was mechanically polished by means of diamond paste of $\sim$1 μm grain size until it showed a mirror-like finish. Thereafter the crystal was mounted (via parallel-running 0.2 mm W wires) to a conventional manipulator which allowed in-situ positioning as well as heating by electron bombardment ($T_{max} \approx 2300$ K) and cooling (via liquid N_2) ($T_{min} \approx 90$ K). The sample temperature was recorded by means of a Re/WRe thermocouple spot-welded to the crystal.

The main cleaning procedure of the Re sample consisted of a few minutes heating in oxygen ($P_{O_2} \approx 10^{-7}$ mbar) at $T = 2300$ K, followed by a short heating to 1500 K in a hydrogen atmosphere ($P_{H_2} \approx 10^{-6}$ mbar) in order to remove residual oxygen. The final removal of carbon and sulfur impurities was achieved by gentle argon ion sputtering and subsequent annealing at 1500 K. The cleaning was continued until there were no longer sulfur and carbon signals detectable in AES and the LEED pattern exhibited bright and sharp diffraction spots on a low background.

2.3. The deposition of aluminum; coverage calibration

Aluminum vapor was supplied by a home-made thermal effusion (Knudsen) cell containing an aluminum oxide (Al_2O_3) crucible loaded with ultrapure (5N) Al (Goodfellows) held at a temperature of $\sim$1050 K, where the Al vapor pressure reaches 10^{-7} mbar [21]. After appropriate outgassing of the source the as-deposited Al films were extremely clean.

In order to check the emissivity, reproducibility and long-term stability of our Knudsen cell, we have exposed our Re sample to Al vapor for definite time intervals and integrated the corresponding Al TD spectra. (We recall that TDS is an ideal tool to determine the total amount of the deposited material and, hence, the relative coverages [25].) The result is shown in Fig. 1, where we

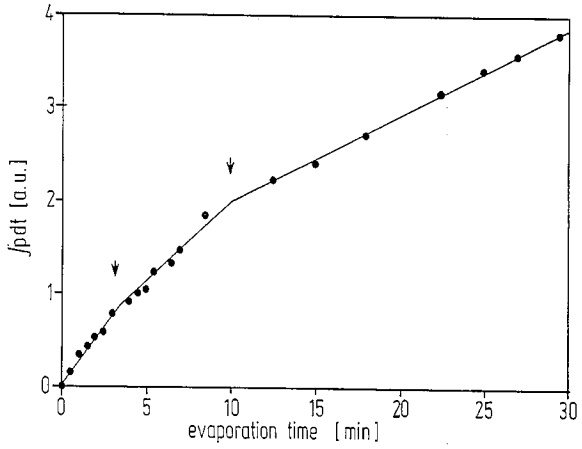

Fig. 1. Plot of the TD peak area $\int P_{Al}dt$ of Al versus the operation time t of the Knudsen cell with the Re substrate held at $T=873$ K. The data points suggest three linear sections which are marked by arrows and indicate the approximate filling of monolayers. Because of the coverage-dependent sticking probability the monolayers are saturated after different time intervals.

have plotted the Al TD peak area versus the operation time t of the Knudsen cell with the Re substrate held at $T=873$ K. The data points suggest three linear sections with decreasing slope (marked by arrows). This behavior could indicate a fairly high (constant) condensation coefficient during the build-up of the first Al monolayer, followed by a somewhat smaller, but also constant, sticking for Al in the second layer and, finally, a third, again lowered, sticking probability for Al on the second layer which then remains practically constant throughout all further coverages investigated. Right after the deposition the sample was cooled to room temperature at a rate of ca. -2 K/s which was high enough to quench the high-temperature morphology of the Al films and the long-range order.

A very important control parameter is the *absolute* coverage of aluminum, Θ_{Al}. We define it in the usual manner as the dimensionless fraction of the number of Al atoms *adsorbed on top of the Re surface* divided by the number of *topmost Re surface atoms* ($=8.127\times10^{-18}$ m^{-2} for the (10$\bar{1}$0) orientation)). Its determination can be pursued by relating the intensity maxima of certain Al-induced LEED structures with the respective thermal desorption peak integrals $\int P_{Al}dt$, provided there exists a reliable or at least plausible real-space structure model and the corresponding Al phase exhibits practically perfect long-range order. As will be shown in more detail in the results section, cf., Section 3.1, the Al atoms form, in the submonolayer range, a p(3 × 1) and a p(2 × 1) LEED phase which suggest *absolute* coverages of $\Theta_{3\times1}=1/3$ and $\Theta_{2\times1}=1/2$, respectively. Actually, the corresponding TD peak integrals are approximately related by 2:3, and we can use the area of the $\Theta_{2\times1}$ TD spectrum as a calibration point for all other relative coverages marking the *absolute* Al coverage of 0.5 at the Al surface concentration of 4.064×10^{18} atoms/m^2. With this calibration we could also quantify the deposition rates of the Knudsen cell: Depending on its operation temperature we could adjust approximate rates ranging from a few Al monolayers per hour to several layers per minute.

3. Results

3.1. Low-energy electron diffraction (LEED)

After appropriate cleaning and annealing the Re(10$\bar{1}$0) surface showed a LEED pattern with very sharp diffraction spots on a low background indicating a chemically clean and crystallographically well-ordered substrate surface. (The chemical cleanliness was also established from our AES measurements reported in Section 3.2.) A representative (1 × 1) LEED pattern of the clean Re surface is reproduced in Fig. 2a.

The deposition of Al was performed with the Re temperature kept fixed. Although we deposited some Al films also at temperatures around 573 K, we adjusted the temperature in most of our experiments to $T\approx873$ K in order to give the Al atoms sufficient mobility to reach the energetically most favorable adsorption sites and to prevent possible contamination of the surface during the deposition runs.

The first noticeable changes in the LEED pattern occur after deposition of about one tenth of a monolayer ($\Theta_{Al}\approx0.10$): we observe diffuse streaks between the Re integer-order beams in the k-direction ([1$\bar{2}$10] direction) which persist and gain intensity upon further deposition until the LEED

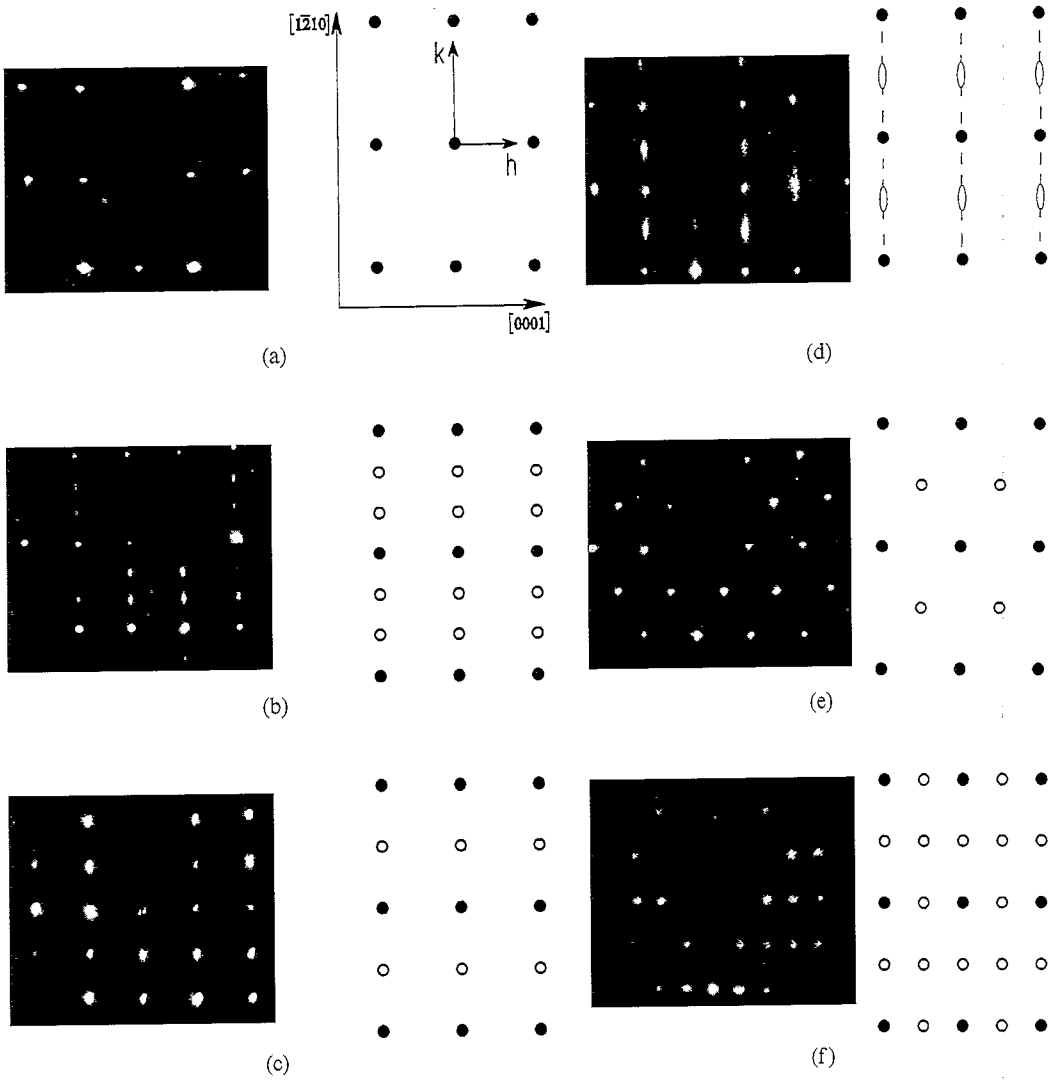

Fig. 2. LEED patterns observed with aluminum on a Re(10$\bar{1}$0) surface prepared by Al deposition at a sample temperature of 735 K; photographs shown on the left, schematic drawings on the right. The lattice vectors are also indicated. (a) LEED pattern of the clean Re(10$\bar{1}$0) surface; electron energy $E_p = 68$ eV. (b) p(3×1) pattern taken at the respective LEED intensity maximum which appears at $\Theta_{Al} \approx 0.3$; electron energy $E_p = 68$ eV. (c) p(2×1) LEED pattern at $\Theta = 0.5$, after a short annealing at 1273 K. The electron energy E_p was 68 eV. (d) "Streaky" (2×1) LEED phase in the coverage interval $0.6 < \Theta_{Al} < 0.9$ showing the transition from the low-coverage (2×1) and the monolayer-coverage (2×1) phase. The electron energy E_p was 80 eV. (e) c(2×2) LEED phase observed in the coverage range $1.5 < \Theta_{Al} < 2.2$. The electron energy E_p was 75 eV. (f) (2×2) LEED pattern formed at a coverage of $\Theta_{Al} \approx 2.6$; $E_p = 75$ eV.

intensity concentrates to sharp spots at $k = \pm 1/3$ and $\pm 2/3$ position leading to the p(3×1) LEED structure shown in Fig. 2b.

Continuation of the Al deposition then leads to a p(2×1) LEED structure in the coverage interval $0.45 < \Theta_{Al} < 0.61$ which is depicted in Fig. 2c. However, as annealing experiments reveal this phase gains its maximum long-range order only after heating to 1373 K. The transition from the p(3×1) to the p(2×1) structure is characterized by a gradual shift of the respective fractional-order beam intensity in the k-direction; under no circumstances is there a coexistence of large (3×1) and (2×1) islands.

Al surface coverages beyond $\Theta_{Al}=0.6$ (up to $\Theta_{Al}\approx 0.9$) introduce considerable disorder as the half-order beams become increasingly blurred and superimposed by relatively sharp streaks in the *k*-direction. This is shown in Fig. 2d. Shortly before the monolayer coverage is reached the streaks disappear and another sharp (2×1) LEED structure (range of stability $0.9<\Theta_{Al}<1.1$) becomes visible which is geometrically identical with the pattern of Fig. 2c, but exhibits a different intensity–voltage (*I–V*) behavior. Beyond $\Theta_{Al}=1.1$, there appears first a very dim and transient (4×4) pattern followed by a much more stable intense $c(2\times 2)$ phase (Fig. 2e) in the coverage range $1.5<\Theta_{Al}<2.2$. Still higher Al concentrations produce a distinct $p(2\times 2)$ structure at $\Theta_{Al}\approx 2.6$ which we reproduce in Fig. 2f. At still higher Al coverages the diffuse background intensity increases, until at $\Theta_{Al}>3.5$ another diffuse $c(2\times 2)$ structure appears which remains visible even for the largest Al depositions investigated.

We conclude this LEED section by saying that the growth of Al in the submonolayer range is characterized by the appearance of discrete superstructures ($p(3\times 1)$ and $p(2\times 1)$) and not by pseudomorphical growth.

3.2. *Auger electron spectroscopy (AES)*

Auger electron spectroscopy with aluminum thin films apparently requires great care because electron-beam effects can easily alter the physical and chemical properties of the films. To our surprise, thermal desorption experiments performed with Al films on Re(10$\bar{1}$0) surfaces irradiated with Auger primary electron beam currents of $\sim 15\ \mu$A revealed a new desorption maximum around 700 K suggesting an artificial electron beam-induced low-energy aluminum binding state. This state could never be seen, if we kept the Auger electron beam current below 10 μA, and this is why we performed our AES experiments only with (defocussed) beam currents of 5 μA and kept the electron exposure as short as possible.

Throughout our AES investigation, we primarily used the Re $N_{6,7}O_{4,5}O_{4,5}$ transition at 33 eV and the Al $L_3M_{2,3}M_{2,3}$ transition at 66 eV which both are situated in the low-energy range with the consequence that the emitted Auger electrons exhibit a similar escape depth of a few monolayers [26].

In Fig. 3, we have plotted the AES intensities of both Al and Re against the aluminum coverage (which was separately determined from the TDS peak integrals, cf. Section 3.3). We know from Fig. 1 that the condensation coefficient of Al on Re is by no means independent of the coverage, and we cannot simply plot the AES intensity versus the Al exposure time in order to obtain the concentration-dependent Al sticking probability. There are several messages in Fig. 3: as expected, the Re AES intensity *de*creases and the Al intensity *in*creases with the ongoing Al deposition. At least in the Re curve, there appears a relatively pronounced change of the slope at $\Theta_{Al}\approx 1$; a second break can be distinguished around $\Theta_{Al}=2$. The occurrence of sudden changes in a signal-intensity versus coverage plot is usually indicative of the completion of a homogeneous deposit layer. We may, therefore, deduce the formation of two practically closed Al layers on top of the Re surface.

Furthermore we notice that the Al Auger signal saturates already after deposition of $\sim$3–4 monolayers, and that the Re Auger signal does not

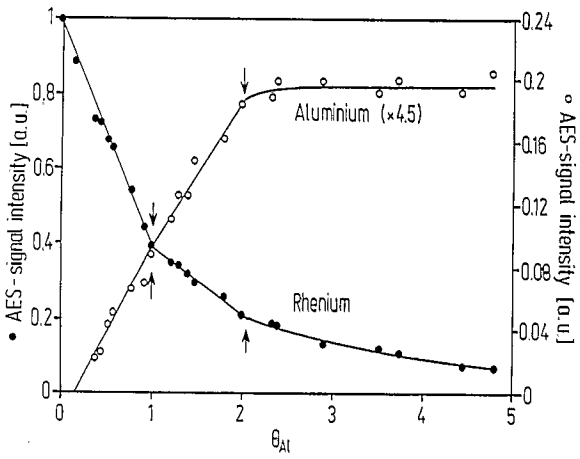

Fig. 3. Plot of the Auger signal intensities of both Al and Re against the aluminum coverage (which was separately determined from the TDS peak integrals, $\int P_{Al}dt$, and the real-space LEED structure models: see text for further details). The deposition temperature was 873 K. There appear two breaks in the slope at coverages of 1 and 2 monolayer(s), respectively, indicating the formation of a closed Al layer.

exactly reach zero. Our TD spectra, on the other hand, prove that the condensation of Al on top of the Re surface still continues (cf. Fig. 5). One can think of at least two explanations for this peculiarity: either, some Re atoms can always diffuse through the Al layers (regardless of their thickness) and will therefore appear in the surface region of the Al film – vice versa, part of the deposited Al atoms may diffuse to the interior of the Re substrate and are hidden from the AES analysis (partial alloying), or (more likely) the growth of Al is governed by the so-called pseudo-Frank–van-der-Merwe mechanism [4,10] where several (say, two or three) complete Al layers are formed (which are still transparent for Re Auger electrons), but larger Al depositions increasingly favor the growth of incomplete islands and/or three-dimensional aggregates. Likewise, the type of growth could also be designated as Stranski–Krastanov (SK) growth (as we can, for larger amounts of deposited material, hardly distinguish the formation of incomplete multilayers or three-dimensional clusters. (Another explanation for the apparent "transparency" of the Al film could be a limited film thickness caused by re-evaporation of the deposited film due to the relatively high substrate temperature of 873 K. However, our Al thermal desorption results reveal desorption maxima only around 1200–1300 K which gives us confidence that we are still far away from the Al adsorption–desorption equilibrium.)

The first possibility, namely diffusion of Re atoms through the Al film, is ruled out by annealing experiments at 1000 K. This temperature is high enough to allow surface migration processes, but too low to thermally desorb Al atoms (cf. Section 3.3). For initial Al coverages $5<\Theta_{Al}<6$ the Re Auger intensity *decreases* upon annealing; and for $\Theta_{Al}>7$ the Re Auger signal actually disappears! This behavior speaks very much against the Re diffusion mechanism as one would, on the contrary, expect an increase of the Re AES signal upon heating. On the other hand, annealing can and certainly will facilitate a transport of Al atoms *parallel* to the surface – depending on the interplay between interfacial and surface free energies and possible kinetic limitations, this surface diffusion can either make an initially rough surface more even, or, on the contrary, support the growth of three-dimensional aggregates of the deposited material. In this latter case, the substrate AES signal should reappear or increase upon annealing, which is not found. AES therefore rather suggests a transport of Al atoms from three-dimensional clusters to fill "holes" in the film.

3.3. Thermal desorption spectroscopy (TDS)

TDS is a very convenient tool to characterize both the binding state(s) and the surface concentration of the deposited material. In Fig. 1, we have already shown the general aluminum "uptake" as measured by TDS, that is, the increase of the deposited amount of Al as a function of the exposure time. In Fig. 4 we now present a typical series of thermal desorption curves, i.e., the amu 27 mass spectrometer signal plotted as a function of the crystal temperature. The measurements were performed with Re samples covered with increasing amounts of Al at $T=873$ K, and the temperature was linearly ramped at a rate of 85 K/s.

Three different Al desorption states can be distinguished. At small coverages there grows a single slightly asymmetric desorption peak in the surprisingly high temperature interval between 1700 and

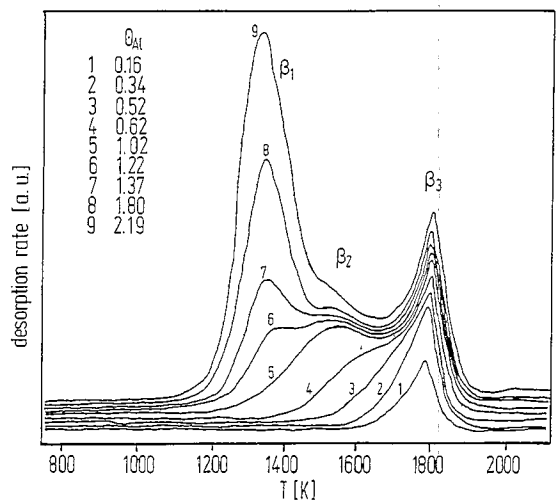

Fig. 4. Series of aluminum thermal desorption spectra (amu 27) from a Re(10$\bar{1}$0) surface covered with increasing amounts of Al at $T\approx873$ K. Clearly, two desorption states β_3 and β_2 can be distinguished which develop with increasing coverage in the submonolayer coverage regime. The temperature was linearly ramped at a rate of 85 K/s.

1900 K ($T_{max}=1800$ K). We denote this maximum as β_3 state. There is almost no temperature shift of the β_3 peak with increasing Θ_{Al} indicating a 1st-order desorption kinetics and a constant Al–Re interaction energy for this state. A second TD maximum begins to grow on the low-temperature tail of the β_3 state already after deposition of $\sim$0.5–0.6 monolayers, i.e., parallel to the formation of the streaky LEED phase and long before the first monolayer saturates. Around $\Theta_{Al}=0.9$ this β_2-state has reached its maximum intensity (curve # 5 in Fig. 4), and is then located at a temperature of $\sim$1540 K. At still larger Al surface coverages a third Al binding state emerges which we assign as β_1-state. It is definitely associated with Al multilayer coverages and dominates the entire desorption spectrum already for coverages $\Theta_{Al}=2$–3. Initially, its peak maximum exhibits a shift towards *lower* temperatures with Θ_{Al}; around $\Theta_{Al}\approx 2$, however, the β_1-peak maximum is, in a small coverage interval, invariant with Θ_{Al}, until it exhibits a slight shift towards *higher* temperatures, i.e. from 1350 to 1430 K, beginning at $\Theta_{Al}\approx 3$, which is indicative of a fractional-order desorption kinetics (caused by preferential desorption from the edges of islands). Fig. 5 displays Al TD spectra for the range $2<\Theta_{Al}<5$. The simple Redhead desorption model which neglects any coverage-dependences [27] can serve to estimate the activation energy for desorption ΔE^* of the individual binding states. If we regard the two states within the first monolayer as independent of each other, assume a 1st-order kinetics and take the preexponential factor as $\nu=10^{13}s^{-1}$, the Redhead analysis reveals $\Delta E^*=440$ (± 5) kJ/mol for the β_3 state and $\Delta E^*=375$ (± 10) kJ/mol for the β_2 state. (If the states do interact with each other, the aforementioned analysis yields at best *approximate* values for the respective activation energies [28,29].) In order to determine the activation energy for desorption of the β_1 state, we apply again the Redhead formalism and arrive at $\Delta E^*=345$ (± 10) kJ/mol for the β_1 state; a value which is a little higher than the heat of sublimation of bulk aluminum ($\Delta H_{sub}=$ 327 kJ/mol [30]) and may perhaps reflect a somewhat strengthened Al–Re interaction in the thin film.

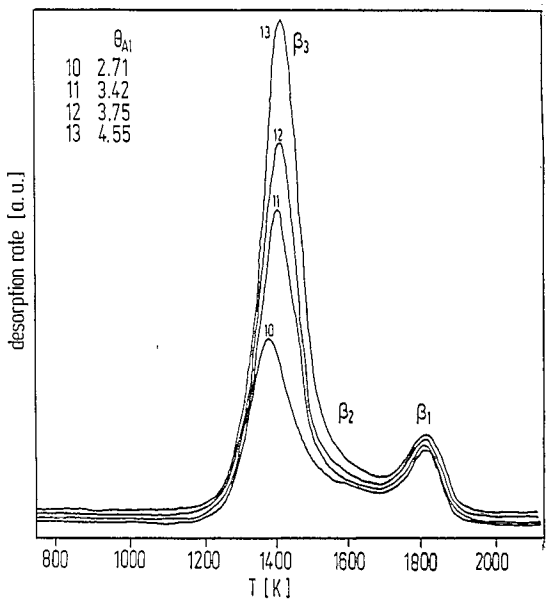

Fig. 5. Al TD spectra for the coverage range $2<\Theta_{Al}<5$, with all other parameters remaining unchanged as compared to Fig. 4. In addition to the β_3 and β_2 states, an intense β_1 state appears which is due to the Al multilayer population.

3.4. Work function change ($\Delta\Phi$) measurements

A short remark illustrates the way we have taken the $\Delta\Phi$ data by means of the Kelvin probe: unlike gas adsorption studies, where $\Delta\Phi$ can be measured continuously during the gas exposure, i.e. without changing the geometry of the Kelvin capacitor, the data can only be taken *discontinuously*, when metal vapors are deposited. Our procedure was as follows. First, the contact potential difference (CPD) between the clean well-ordered Re(10$\bar{1}$0) surface and the inert Au reference electrode was measured and the respective $\Delta\Phi$ taken as a reference guideline. Note that the Kelvin method does not provide *absolute* values, but rather *relative* work function differences (unless one knows the absolute work function of either the reference electrode or the clean sample). By moving the Re sample back and forth the reference electrode of the Kelvin probe and readjusting the distance between the sample and the reference electrode to within ± 0.1 mm we attained a reproducibility of the work function signal better than 20 meV. Thereafter, we moved the Re sample in front of the Knudsen cell, deposited a well-defined amount of Al, readjusted it in

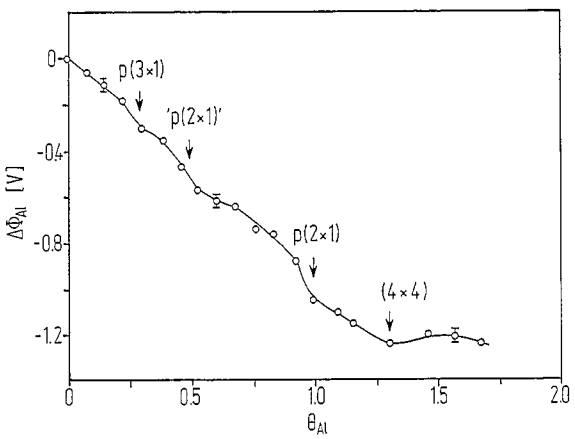

Fig. 6. Coverage (Θ)-dependence of the Al-induced work function change of the Re(10$\bar{1}$0) surface as measured by the Kelvin method at 300 K. The ranges of stability of the various Al-induced LEED phases are indicated in the figure. Within the limits of accuracy, a steady decrease down to $\Delta\Phi \approx -1.2$ eV at saturation is measured ($\Theta_{Al} \approx 1.5$ ML).

front of the vibrating Kelvin reference electrode. The contact potential difference with respect to the clean surface (1st measurement!) was taken as the Al-induced $\Delta\Phi$, before all deposited Al was thermally desorbed in order to restore the clean Re(10$\bar{1}$0). This procedure was applied for each data point of Fig. 6 which displays the Θ dependence of the Al-induced work function change. For convenience, we have also indicated the ranges of stability of the various Al-induced LEED phases. Within the limits of accuracy (the data points exhibit some scatter), we find a steady decrease of $\Delta\Phi$, until at $\Theta_{Al} \approx 1.5$ the saturation value ($\Delta\Phi \approx -1.2$ eV) is reached. If we reference this value to the work function Φ_0 of the clean Re(10$\bar{1}$0) surface (=5.20 eV [31]) we determine the work function of the two-layer Al film as 4.0 eV. If we now regard the Al adatoms as an array of electrical dipoles of density σ and apply the Helmholtz equation $\mu_0 = \mu_0\sigma/\varepsilon_0$ in order to determine the initial dipole moment μ_0, we arrive at $\mu_0 \approx 0.29$ debye which is relatively small as compared to dipole moments typical for alkali metal adsorption ($\mu_0 > 5$ D).

4. Discussion

We will subdivide the discussion into two parts: First, we consider the (submonolayer) coverage range $0 < \Theta_{Al} < 1$ which is dominated by a "chemical" interaction between the Al adatoms and the substrate. The second part comprises all features of the multilayer regime including the aluminum film growth mechanism. Both regimes are characterized by strong Al–substrate and Al–Al interactions both of which seem to be responsible for the thermal desorption states and, hence, the binding energetics as well as for the occurrence of the ordered LEED phases, i.e., the geometry of the local adsorption site *and* the long-range order.

4.1. The submonolayer coverage regime ($0 < \Theta_{Al} < 1$)

4.1.1. The p(3 × 1) and (2 × 1) LEED phases

In the following section, we will summarize the LEED features and propose possible real-space structure models for the p(3 × 1) and (2 × 1) phases, which are, as mentioned above, essential for a correct absolute Θ_{Al} evaluation and will discuss the details of the chemical interaction between the Al atoms and the Re surface which is, among others, reflected in the binding states of the TD spectra and the Al-induced work function change.

We recall from Section 3.1 that for coverages $\Theta_{Al} < 0.3$ streaks in [0001] direction are observed in LEED. For $\Theta_{Al} \geq 0.3$ these streaks concentrate and sharpen to distinct spots of a p(3 × 1) structure. This behavior can be attributed to the operation of attractive interactions in [0001] and repulsive interactions in the perpendicular [1$\bar{2}$10] direction of the Re(10$\bar{1}$0) surface. At very small coverages strings of Al atoms in [1$\bar{2}$10] direction are formed which are most likely located in the troughs of the Re(10$\bar{1}$0) surface. The relatively sharp streaks thereby indicate an already pronounced long-range order in [0001] direction, while disorder still prevails in the perpendicular [1$\bar{2}$10] direction, that is, the chains are statistically shifted with respect to a Re lattice vector. As the Al coverage approaches $\Theta_{Al} = 0.3$, the chains lock into periodic positions also in this direction resulting in the sharp (3 × 1) LEED pattern of Fig. 2a. It is very likely that the Al atoms occupy the fourfold coordinated sites inside the troughs of the Re surface. This is illustrated in Fig. 7a. Clearly, the (indicated) unit mesh contains three Re surface atoms and a single

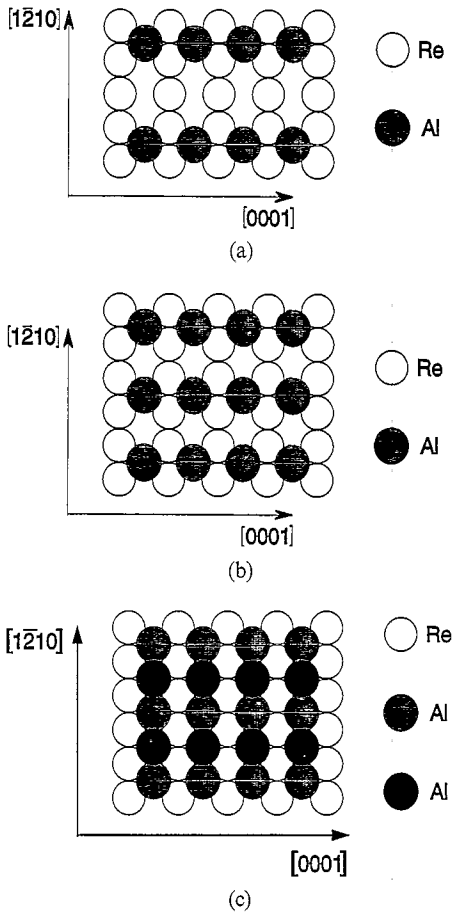

Fig. 7. Tentative real-space (structure) models for the various Al-induced LEED superstructures based on the metallic radii of Al and Re and the assumption of a maximum coordination. (a) (3×1) Al phase at $\Theta=0.3$, whereby the Al atoms occupy the fourfold coordinated sites inside the troughs of the Re surface. The (indicated) unit mesh contains three Re surface atoms and a single Al atom, and the nominal coverage associated with the (3×1) structure is 0.33. (b) Structure model for the (2×1) structure observed at an Al surface coverage of 0.5. In [0001] direction, the Al atoms retain the spacings of the former (3×1) phase, but in [1$\bar{2}$10] direction every second trough site is occupied by an Al atom. Note that annealing at 1000 K is required to introduce maximum long-range order. (c) Structure model suggestion for the (second) (2×1) LEED phase observed at $\Theta_{Al}\approx1$ ML (range of stability $0.9<\Theta_{Al}<1.1$). This model assumes the exclusive occupation of sites inside the troughs of the Re surface. However, in order to accommodate as many Al atoms as there are Re atoms despite the Re–Al misfit every second Al atom must become somewhat displaced normal to the surface; the respective Al atoms are indicated in Fig. 7c by a darker colour.

Al atom, and the nominal coverage associated with the (3×1) structure is 0.33. [We refer again to Section 2.3 and emphasize that this coverage is consistent with the coverage assignment $\Theta_{Al}=0.5$ for the subsequent (2×1) structure (see below) in that the corresponding Al TDS peak areas are related by 2:3]. The dimensions of the atoms chosen in Fig. 7 are based on the *metallic* radii of both Re and Al, for reasons explained below.

We emphazise that this model (as all other structure suggestions of this work) is only tentative and does not allow final conclusions on the real-space structure (whose quantitative determination requires a dynamical LEED structure analysis). Furthermore, for the sake of simplicity, we attribute all Al superstructures to *true* Al phases with long-range order and explicitly neglect any possible Al-induced surface reconstruction effects (for which we do not have hints from our experiments).

In any structure model, a crucial parameter is the physical size of the adatoms which in turn is determined by their electronic configuration. Although our $\Delta\Phi$ measurements indicate a certain donation of charge from an Al adatom to the Re substrate this charge transfer should not make an individual Al atom shrink considerably upon adsorption. In recent measurements of alkali metal (Na, K) adsorption on gold (100) we observed much larger decreases of the work function, but all experimental data could be interpreted consistently by using the metallic and not the ionic radii [34]. The metallic radius of an Al atom is 1.432 Å, its ionic radius (Al^{3+}) is given by Pauling [35] as 0.5 Å, and its "monovalent" radius (Al^{+}) as 0.72 Å. From our $\Delta\Phi$ measurements we could deduce the initial dipole moment μ_0 to be $\sim$0.29 debye which in turn provides a rough estimate of the amount of charge transferred from an Al atom to the Re substrate: this charge turns out to be merely 3% of the elementary charge e_0 and rules out significant ionic bonding contributions. This gives us confidence that $r_{Al}=1.43$ Å is a realistic assumption for our structure model considerations. A close similarity with other adsorption systems should be underlined here. The adsorption of lithium on W(211) [36] and barium on Mo(211) [37] reveals similar structures in that chain-like arrangements are formed perpendicular to the furrows of the

anisotropic surfaces which originate from the operation of repulsive forces in the direction parallel to the troughs and attractive interactions in the perpendicular direction across the troughs. Because of the relatively small effective charge located on an Al adatom "direct" electrostatic effects can certainly be neglected, and the origin of the long-range interactions responsible for the ordering must be sought in the so-called "through-bond" contributions whose origin is quantum-mechanical (sharing of bonding electrons by adjacent atoms), whereby the character of these interactions can be repulsive and/or attractive [38]. Experiments show that their operational range can extend up to 10 Å [39] which is clearly sufficient to explain the (3×1) periodicity observed in our case, with its relatively extended unit mesh.

Before we focus on the next structure formed, the $p(2\times1)$ phase, the transition from the $p(3\times1)$ to the (2×1) between $\Theta_{Al}=0.33$ and 0.45 deserves attention, and the observed LEED features, namely the gradual shifts of the extra-spot intensity maximum from $k=1/3$ and 2/3 to $k=1/2$ positions can, in the first instance, be explained by a statistical mixture of $p(3\times1)$ and $p(2\times1)$ unit cells whose composition varies continuously with the Al surface concentration [40,41]. Gradmann has given a simple analytical explanation for the occurrence of such coverage-dependent shifts, based on the given surface anisotropy and the assumption of anisotropic interaction forces [42]. Unfortunately we did not scrutinize the coverage-dependence of the fractional-order LEED beams, but one may assume a linear relationship as a first approximation.

Another explanation considers a two-step process consisting of the complete melting of the (3×1) phase and the subsequent formation of (2×1) islands which are quite extended in [0001]-direction but very narrow in the perpendicular $[1\bar{2}10]$ direction: Spot-splitting may then be produced by antiphase boundaries between adjacent islands (normal to the direction of the antiphase boundary) as was shown by McKee et al. [43]. However, in order to obtain a sharp (2×1) pattern (without split-spots or streaks) the antiphase boundaries must be removed which may require substantial correlated surface diffusion and, hence, a high mobility of the adsorbed Al atoms. A process of this kind may be supported by our observation whereafter annealing at elevated temperatures leads to a sharp (2×1) LEED pattern without streaks. The well-developed (2×1) structure (cf. Fig. 2b) corresponds to an Al surface coverage of 0.5, and a reasonable real-space structure model is shown in Fig. 7b. In the [0001] direction, the Al atoms retain the spacings of the former (3×1) phase, but in the $[1\bar{2}10]$ direction, i.e., parallel to the troughs, they now exhibit twice the periodicity of the Re atoms. The Al–Al distances are 4.458 Å in the [0001] direction and 5.520 Å in the $[1\bar{2}10]$ direction, which leads to an overall surface-density of $\sigma_{2\times1}=4.064\times10^{18}$ atoms/m^2. With regard to the local geometry of the adsorption site of the (2×1) structure, we emphasize that the sites most likely remain unchanged compared to the (3×1) structure, i.e. the Al atoms continue to occupy the quasi-fourfold coordinated trough positions.

Next we consider the situation for Al coverages $\Theta_{Al}>0.5$. The structure model of Fig. 7b suggests that an increase of the Al surface concentration beyond this value should lead to a continuous adsorption of Al atoms *inside* the troughs, and the corresponding mutual distances of the Al atoms in the $[1\bar{2}10]$ direction should shrink accordingly, until the Al atoms can again lock in periodic positions. Note, however, that the radius of an Al atom is 4.5% larger than that of a Re atom. While it is not difficult to accommodate half a monolayer of Al atoms periodically in *equivalent* positions in $[1\bar{2}10]$ direction in the troughs (their mutual distance then is still twice the Re atom diameter) problems arise for coverages larger than $\Theta_{Al}=0.5$: in this case a certain fraction of Al atoms can no longer be accommodated in *equivalent* sites inside the troughs, and the rigid geometrical correlation between the Al atoms the Re atoms in $[1\bar{2}10]$ direction is lost. This is exactly what we observe: a LEED pattern with sharp streaks in $[1\bar{2}10]$ direction for coverages $0.6<\Theta_{Al}<0.9$ indicating one-dimensional disorder in $[1\bar{2}10]$ direction. The sharpness of the streaks in [0001] direction thereby demonstrates that the "channels" of the $(10\bar{1}0)$ surface still remain the most favored location for the adsorbing Al atoms.

In another (but equivalent) view, one may attribute the streaks to the formation of one-dimensional incommensurate structures (as was proposed for the already cited system Li/W(211) [36]). One-dimensional incommensurate structures can either result in streaky LEED patterns (if the adatoms and substrate atoms are out of phase) or in complex diffraction patterns with extended unit meshes. In their work on alkali-metal adsorption on Ni(110) [44,45], Gerlach and Rhodin formulated three conditions for the appearance of one-dimensional incommensurate structures: (i) the substrate must possess a two-fold rotational symmetry in conjunction with an atomic anisotropy (channels, for example), (ii) the adatoms and the substrate atoms must exhibit a different size, and (iii) the interaction energy between the adsorbate atoms must be appreciable and govern the occupation of the adsorption sites. Clearly, all these requirements are fulfilled in our case.

4.1.2. The structure of the (2 × 1) LEED phase at $\Theta_{Al}=1$

We recall that a trough of the Re(10$\bar{1}$0) surface can hardly accommodate as many Al atoms as there are Re atoms (due to the 4.5% larger diameter of the Al atoms), and a true (1 × 1) structure at $\Theta_{Al}=1$ cannot be formed. Nevertheless, we find a pronounced long-range order around $\Theta_{Al}=1$ reflected by the appearance of a sharp (2 × 1)-LEED pattern. The relatively small misfit does indeed not allow to form a linear chain of Al atoms inside a Re trough, but if every second Al atom in [1$\bar{2}$10] direction is slightly displaced perpendicular to the surface, all Al atoms can still be accommodated in such a trough. The resulting configuration of slightly sinusoidally bent chains of Al atoms with a period length of twice the Re–Re distance along the [1$\bar{2}$10] direction could easily explain the observed (2 × 1) periodicity, and a respective structure model is shown in Fig. 7c. By surface crystallography, this corrugated top Al layer should then contain the same number of atoms per unit area as the Re(10$\bar{1}$0) surface, namely, $\sigma_{2\times1'}=8.13\times10^{18}$ Al atoms/m^2, which is much less than the characteristic surface density of the Al(110) face (= 8.66×10^{18} m^{-2}).

All in all, we arrive at a morphology of the Al layer which very much resembles the surface structure of the Re(10$\bar{1}$0) surface except for a slight perpendicular corrugation (which is probably less than 0.4 Å as a simple geometric consideration shows). Nevertheless, the Al atoms which are displaced away from the surface do not exhibit the same favorable coordination with respect to the adjacent Re atoms as the Al atoms closer to the surface, and this could explain the appearance of the β_2 state observed in the thermal desorption spectra just around $\Theta_{Al}\approx1$ as pointed out further below.

Apparently at this stage of Al deposition the strongly corrugated Re substrate entirely governs the morphology of the monoatomic Al film at $\Theta_{Al}=1$. A similarly "open" array of adatoms has been reported also for the systems Ag and Cu on tungsten (100) surfaces [10,46]: especially in the Cu/W(100) case repulsive interactions between adjacent Cu atoms were invoked to account for the absence of close-packed layers. We may also compare the structure of our monolayer Al film with the observations reported for Al on Mo(110) and Ta(110) [19–21], whereafter the Al atoms form two-dimensional arrays with their own periodicity, independent of the structure of the host lattice. However, the situation is different there, because both (110) surfaces represent the most densely packed surface of the bcc lattice and exhibit a minor structural corrugation only, quite in contrast to the Re(10$\bar{1}$0) face which possesses deep potential energy minima resulting in a strong influence on the position of the adsorbing Al atoms.

4.1.3. The binding state of Al in the submonolayer coverage range

We turn now to a brief discussion of the Al binding states observed in the submonolayer range as revealed by the thermal desorption and work function results. Interesting and somewhat unusual for deposition of metals on metals is the presence of two different binding states in the submonolayer coverage regime which is rather typical for gas adsorption on metals. However, with Na and K adsorption on Au(100) we have recently also observed several binding states and attributed to a coverage-dependent change in the bonding character from a largely ionic to a rather metallic state

[34]. We recall that different binding states within the monolayer coverage may either reflect a so-called a priori surface heterogeneity in that geometrical adsorption sites of different energy are sequentially occupied by ad-atoms (this case is normally found with corrugated and rough surfaces), or they may indicate an a posteriori heterogeneity induced by the adatoms themselves which exert mutual repulsive interaction forces as their concentration increases. In the present case of Al on Re(10$\bar{1}$0), we think that both explanations are applicable, although the inherent corrugation of the (10$\bar{1}$0) surface certainly is a dominating factor. A comparison between the LEED and TDS features of the submonolayer regime reveals that the first state (β_3) develops parallel to the first (2×1) LEED phase, and we may associate it with the occupation of the quasi-fourfold coordinated trough sites of Fig. 7. It is not until the streak phase forms for $\Theta > 0.6$ that the β_2 state grows in, and it may well reflect the occupation of less coordinated and energetically less favorable trough sites pointed out in Section 4.1.2. In addition, the larger packing density of the Al atoms may cause additional repulsive interactions which alone could account for the lower binding energy of the split-off state. As pointed out in Section 4.1.1 these repulsions are due rather to through-bond interactions than to being produced by direct electrostatical forces. This is in contrast to the alkali-metal case, where large work function changes up to several eV are the rule and the decrease in binding energy is dominated by dipole–dipole interactions. On the other hand, the Al-on Re-system is also different from the frequently studied noble metal adsorption on transition metal surfaces, where $\Delta\Phi$ is quite small and seldom exceeds a few hundred meV indicating a vanishing charge transfer between adatom and substrate. Another fairly surprising result is that the two-layer Al film practically exhibits the work function of the Al(110) surface ($\Phi_{Al(110)} = 4.06$ eV [33]; for comparison: $\Phi_{Al(111)} = 4.26$ eV [32] and $\Phi_{Al(100)} = 4.41$ eV [33]), despite its completely different structure with a $\sim 6.5\%$ lower packing density.

Although the bonding situation calls for a fundamental quantum-chemical treatment of the Al "chemisorption" on Re (which has not been performed so far) there are much simpler empirical models available based on thermodynamical considerations which can successfully describe the overall energetics. Miedema and Dorleijn [30] have developed a semi-empirical theory based on surface free energy considerations to predict adsorption energies for a metal A on a metal B. They treat the adsorbed atoms A simply as little pieces of metals, whose heat of adsorption can be evaluated based on the molar surface area of the adatom, the specific free surface energies of the two metals at 0 K and the heat of solution of metal A in metal B. It is remarkable in this context that they arrive at an Al–Re adsorption energy of 465 kJ/mol which is surprisingly close to our experimentally determined value of 440 kJ/mol.

4.2. *The multilayer coverage regime ($\Theta_{Al} > 1$)*

Next we consider Al surface concentrations which exceed the monolayer coverage ($\Theta_{Al} = 1$), and we refer to this situation simply as the "multilayer" regime. For the coverage regime $1.5 < \Theta_{Al} < 2.2$ we basically observe the formation of a stable $c(2\times2)$ LEED pattern which entirely dominates the second Al layer; at the same time, a new thermal desorption state (β_1) appears in the TD spectra. In order to develop a realistic structure model for the $c(2\times2)$ phase we have taken the surface structure of the foregoing (2×1) structure at $\Theta = 1$ and simply continued by "filling in" the additional Al atoms in sites with the highest coordination possible – this results in an occupation of the (slightly corrugated) trough sites of the first Al layer, whereby the Al atoms of the second layer are located in a short bridge site provided by two Re row atoms underneath and in a long-bridge site made up of the Al atoms of the first layer: in this configuration, the second-layer Al atoms have a direct neighbor in [0001] direction, i.e., on the left and on the right site. However, this simple continuation of the trough-site occupation would lead to the formation of deep (corrugated) troughs between the adjacent (corrugated) rows of top-layer Al atoms. This situation must be considered energetically unfavorable, and the whole system of first and second layer Al atoms undergoes a *relaxation* process. This can either consist of a mutual

shift of entire adjacent Al rows by half a Re lattice vector in $[1\bar{2}10]$ and $[\bar{1}2\bar{1}0]$ direction, respectively, or simply an alternating buckling of the Al atoms within adjacent rows. Consequently, the positive displacements of adjacent top-layer Al rows become "staggered" with respect to each other which could account for the c(2×2) symmetry of the LEED pattern. Our respective (tentative) structure model suggestion is presented in Fig. 8.

Due to the aforementioned relaxation, both the influence of the Re substrate (which is strongly corrugated in [0001] direction) and the misfit between the Re and Al atomic diameters (which led to a corrugation in $[1\bar{2}10]$ direction) can gradually be attenuated as the Al film thickness increases. Our LEED results indicate the formation of a (2×2) structure for the third layer ($\Theta_{Al} > 2.2$), and in terms of our relaxation model this would mean that merely every second Al atom in $[1\bar{2}10]$ and [0001] direction is displaced in (+) or in (−) direction perpendicular to the surface.

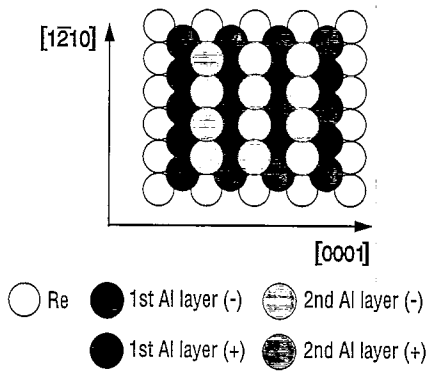

Fig. 8. Tentative structure model for the c(2×2) LEED pattern formed at $\Theta_{Al} \approx 2$. This model is practically a continuation of the real-space (2×1) structure proposed for the saturated monolayer (cf. Fig. 7c) in that another Al monolayer is accommodated by adsorption of additional Al atoms in the troughs along $[1\bar{2}10]$ direction. To provide the c(2×2) symmetry, a relaxation of the Al atoms must be assumed to yield a "staggered" buckling of adjacent rows of Al atoms which adsorb in the troughs of the first layer. This buckling is indicated in Fig. 8 by a different grey coloration of the top layer atoms. The (+) mark denotes all Al atoms which stick somewhat out of the hypothetical second-layer surface plane; the Al atoms indicated by the (−) sign are located somewhat below this plane.

Note that all these layers regardless of whether they exhibit a (2×2) or a c(2×2) periodicity, are somewhat corrugated. As pointed out above, this buckling is a consequence of both the inherent corrugation of the hcp $(10\bar{1}0)$ surface and the misfit between Al and Re. The latter is large enough to prohibit a compression of the Al atoms adsorbed in the troughs along $[1\bar{2}10]$ direction. If such a compression occurred, the Al layer would exhibit the same lattice as the Re substrate, and *pseudomorphical* growth of aluminum would result. This is, however, not the case, and the overall situation seems to represent a compromise between the geometrical reality of the too narrow Re–Re distances of the substrate and the tendency of the Al adatoms to adsorb in highly coordinated sites. If our structural assumptions are correct both the first and the second Al layer contain the same number of Al atoms, viz., $n_1 = n_2 = 8.12 \times 10^{18}$ m^{-2}. This agrees well with the AES results which showed the completion of the first and the second monolayer at the same coverage (cf. Fig. 3).

As more Al layers grow on top of this "diluted" bilayer, relaxation processes increasingly take place within the subsequent layers thereby causing the observation of an intermediate p(2×2) phase, followed by a fairly stable c(2×2) pattern which remains visible up to the deposition of 8 to 10 nominal Al monolayers.

As pointed out by one of the referees [47] there is a common tendency of epitactically growing fcc metals to form dense packings with (111) orientation. The observed final c(2×2) structure could then be explained by a distorted (unaxially compressed or elongated) fcc Al layer with approximate (111) orientation, and the transformation from (distorted) Al bilayers right at the interface to the (practically densely packed) epitactic Al bulk crystal could be understood in a straightforward manner.

However, the appearance of discrete LEED superstructures even at Al coverages > 3 ML proves the stability of the corrugated or distorted Al film and underlines *that the structure and anisotropy of the Re substrate largely determines the growth and geometry of the deposited Al films* also in the multilayer regime. This is in line with

previous work where Ag [48] and Au films [49] were grown on the (geometrically quite similar) Ru(10$\bar{1}$0) substrate and showed the same strong influence of the substrate geometry on the film morphology.

A final comment concerns also the type of growth which we can deduce for the multilayer regime from our combined LEED, AES, and TDS measurements. Provided that there occur no temperature-induced alloying effects (which could easily modify or change the features of the thermal desorption spectra [17]) we may come to the following conclusions. As noted in Section 3.3, the temperature position of the β_1 state is only slightly dependent on Θ_{Al}; roughly, the desorption process obeys a first-order kinetics. Only for $\Theta_{Al} > 3$, the TD peak shifts somewhat towards *higher* temperatures. Normally, one would expect a zero-order kinetics for desorption from a thick condensed layer of metal deposit, which means that the TD peaks possess a common leading-edge on their low-temperature tail. The different situation for the Al/Re(10$\bar{1}$0) system can be explained on the basis of our structure model(s) as follows. For $1 < \Theta_{Al} < 2$ those Al atoms which are adsorbed on top of the first layer are still in some contact with the Re atoms underneath, due to the relatively open packing of the first-layer Al atoms. The corresponding chemisorption energy (which is assumed equal to the activation energy for desorption) is therefore somewhat smaller than for the Al atoms within the first layer (they have optimum contact with the Re substrate which is energetically reflected by the β_3 and β_2 state), but the respective desorption energy is still larger than the enthalpy of sublimation of bulk Al. For the third and following layers (up to the ~10th layer) this enhancing influence of the substrate with respect to the binding energy becomes increasingly reduced which explains the apparent change of the desorption kinetics (as well as of the desorption energy, which more and more approaches the value of the sublimation enthalpy of Al as pointed out in Section 3.3).

According to surface thermodynamics [10], the type of growth of metallic thin films is governed by the energy balance Δ between the surface free energies γ_s and γ_f of the substrate and the film, respectively, and the interface energy γ_i at the boundary of the two metals:

$$\Delta = \gamma_i + \gamma_f - \gamma_s .$$

This criterion allows a rough distinction between the three most abundant types of growth: If $\Delta \leqslant 0$, Frank–van der Merwe (layer-by-layer) growth [50] or Stranski–Krastanov growth [51] (first layer complete, then three-dimensional islands) is predicted, while for $\Delta \geqslant 0$ the so-called Volmer–Weber growth [52] (only three-dimensional islands) should prevail. Despite this clear thermodynamical rule an exact prediction of the growth is difficult, for two reasons. First, the above relation does not at all consider any kinetic limitations, and, second, the exact determination of the interfacial energy γ_i is difficult. Miedema and Dorleijn [30] have given a formula which allows an estimation of γ_i:

$$\gamma_i \approx \left(\sqrt{\gamma_f} - \sqrt{\gamma_s} \right)^2 .$$

and with $\gamma_{Al} = 1.20$ J/cm^2 and $\gamma_{Re} = 3.65$ J/cm^2 we arrive at a negative value for the quantity Δ which in turn predicts a wetting of the surface leading to either SK or FM growth. Our LEED and Auger data support this prediction, in that they suggest the formation of at least two closed Al monolayers, on top of which either (incomplete) Al layers or large and rather three-dimensional Stranski–Krastanov crystallites grow. Admittedly, a distinction between these two cases solely on the basis of LEED and AES and, hence, a clear-cut determination of the actual growth mechanism is, therefore, not possible here. Unfortunately, there was no scanning tunneling microscope available at the time of our study, and we could not check our (indirect) conclusions in real space. However, a separate STM investigation of the growth of Al on Re is planned for the future.

This study can then also shed light on the question whether or not *alloying* and/or interdiffusion effects between Al and Re will occur. Our present work can only contribute a little to this problem as there was no probe with atomic reso-

lution available, although it does not explicitly support the alloying hypothesis. As mentioned in the Introduction, alloying effects could be ruled out for Al on Ta(110) and Mo(110) [21], but were definitely found for Al on Ru(0001) [17,18]. Therefore the high cohesive energy of these metals cannot be the decisive factor for alloying or non-alloying. The crystallographic orientation of a given surface seems to be irrelevant here either, since the densely-packed bcc (110) surfaces do not favor alloying, but the also densely-packed hcp (0001) surfaces do, while the crystallographically "open" hcp (10$\bar{1}$0) surface of Re (our work) does not particularly facilitate heavy alloying processes.

Acknowledgements

This work was generously supported by the Deutsche Forschungsgemeinschaft (SFB 290) and the Fonds der Chemischen Industrie. We thank Dr. E. Schwarz for many fruitful discussions and K. Schubert and R. Cames for technical assistance.

References

[1] See, for example: Thin Metal Films and Gas Chemisorption, Ed. P. Wissmann, Vol. 32 of Studies in Surface Science and Catalysis (Elsevier, Amsterdam, 1987).
[2] C.M. Schneider, P. Bressler, P. Schuster, J. Kirschner, J. de Miguel and R. Miranda, Phys. Rev. Lett. 60 (1990) 1059.
[3] F. Gauthier and D. Stoeffler, Surf. Sci. 249 (1991) 265.
[4] E. Bauer, Ber. Bunsenges. Phys. Chem. 95 (1991) 1315.
[5] J.A. Venables, Surf. Sci. 299/300 (1994) 798.
[6] M. Gebhardt, in: Crystal Growth: An Introduction, Ed. P. Hartmann (North-Holland, Amsterdam, 1973) ch. 3.
[7] E.M. Savitskii, M.A. Tylkina and K.B. Kovarova, Russ. J. Inorg. Chem. 6 (1961) 1003.
[8] (a) D.R. Short, S.M. Khalid, J.R. Katzer and M.J. Kelley, J. Catal. 72 (1981) 288.
(b) V. Haensel, in: Heterogeneous Catalysis: Selected American Histories, Eds. B.H. Davis and W.P. Hettinger, Jr., ACS Symp. Ser. 222 (1983) 141.
[9] Chemiker-Kalender, Ed. H.U. Vogel (Springer, Berlin, 1966) p. 121.
[10] For a review see: E. Bauer, Appl. Surf. Sci. 11/12 (1982) 479.
[11] (a) E. Bauer, F. Bonczek, H. Poppa and G. Todd, Surf. Sci. 53 (1975) 87;
(b) E. Bauer, H. Poppa, G. Todd and F. Bonczek, J. Appl. Phys. 45 (1974) 5164.
[12] M. Mundschau, E. Bauer, W. Telieps and W. Swiech, Surf. Sci. 213 (1989) 381.
[13] J. Kołaczkiewicz and E. Bauer, Surf. Sci. 175 (1986) 508.
[14] M. Tikhov and E. Bauer, Surf. Sci. 203 (1988) 423.
[15] R. Bergholz and U. Gradmann, J. Magn. Magn. Mater. 45 (1984) 389.
[16] J.A. Rodiguez, R.A. Campbell and D.W. Goodman, J. Vac. Sci. Technol. A 10 (1992) 2540.
[17] C.T. Campbell and D.W. Goodman, J. Phys. Chem. 92 (1988) 2569.
[18] Y. Wu, H.-S. Tao, E. Garfunkel, T.E. Madey and N.D. Shinn, Surf. Sci. 336 (1995) 123.
[19] A.G. Jackson and M.P. Hooker, Surf. Sci. 28 (1971) 373.
[20] J. Kołaczkiewicz, M. Hochół and S. Zuber, Surf. Sci. 247 (1991) 284.
[21] A.G. Jackson, M.P. Hooker and T.W. Haas, J. Appl. Phys. 38 (1967) 4998.
[22] See, for example: F.N. Bradley, Materials for Magnetic Functions (Hayden, New York, 1971) p. 138.
[23] M. Parschau and K. Christmann, Ber. Bunsenges. Phys. Chem. 99 (1995) 1376.
[24] D'Ans-Lax, Taschenbuch für Chemiker und Physiker, 3 Aufl. (Springer, Berlin, 1967).
[25] K. Christmann, Introduction to Surface Physical Chemistry (Steinkopff, Darmstadt, 1991) p. 152 ff.
[26] M.P. Seah and W.A. Dench, J. Surf. Interface Anal. 1 (1979) 2.
[27] P.A. Redhead, Vacuum 12 (1962) 203.
[28] D.L. Adams, Surf. Sci. 42 (1974) 12.
[29] P.W. Tamm and L.D. Schmidt, J. Chem. Phys. 51 (1969) 5352; 54 (1971) 4775.
[30] A.R. Miedema and J.W. Dorleijn, Surf. Sci. 95 (1980) 447.
[31] U. Muschiol, personal communication.
[32] J. Hölzl and F.K. Schulte, Vol. 85 of Springer Tracts in Modern Physics (Springer, Berlin, 1979).
[33] H.B. Michaelson, J. Appl. Phys. 48 (1977) 4729.
[34] A. Neumann, S.L.M. Schröder and K. Christmann, Phys. Rev. B 51 (1995) 17007.
[35] L. Pauling, Die Natur der chemischen Bindung, 2nd ed. (Verlag Chemie, Weinheim, 1964) Table 13.3, p. 475.
[36] V.K. Medvedev, A.G. Naumovets and T.P. Smereka, Surf. Sci. 34 (1973) 368.
[37] V.K. Medvedev and I.N. Yakovkin, Sov. Phys. Solid State 23 (1981) 379.
[38] T.B. Grimley, Proc. Phys. Soc. London 92 (1967) 776.
[39] D.L. Adams and L.H. Germer, Surf. Sci. 27 (1971) 21.
[40] L.H. Germer, J.W. May and R.J. Szostak, Surf. Sci. 7 (1967) 430.
[41] G. Ertl and J. Küppers, Surf. Sci. 21 (1970) 61.
[42] U. Gradmann, Ann. Phys. (Leipzig) 26 (1971) 283.
[43] C.S. McKee, D.L. Perry and M.W. Roberts, Surf. Sci. 39 (1973) 176.
[44] R.L. Gerlach and T.N. Rhodin, Surf. Sci. 10 (1968) 446.
[45] R.L. Gerlach and T.N. Rhodin, Surf. Sci. 17 (1969) 32.

[46] E. Bauer, H. Poppa, E. Todd and P.R. Davis, J. Appl. Phys. 48 (1977) 3773.
[47] We are grateful to one of the referees for having drawn our attention to this point.
[48] P. Lenz-Solomun and K. Christmann, Surf. Sci. 345 (1996) 41.
[49] S. Poulston, M. Tikhov and R.M. Lambert, Surf. Sci. 331–333 (1995) 818.
[50] F.C. Frank and J.H. van der Merwe, Proc. R. Soc. London A 198 (1949).
[51] I.N. Stranski and L. Krastanov, Ber. Akad. Wiss. Wien 146 (1938) 797.
[52] M. Volmer and A. Weber, Z. Phys. Chem. 119 (1926) 277.